frontiers | Frontiers in Nuclear Engineering

TYPE Original Research
PUBLISHED 05 August 2025
DOI 10.3389/fnuen.2025.1599740



OPEN ACCESS

EDITED BY
Yuh-Ming Ferng,
National Tsing Hua University, Taiwan

REVIEWED BY
Jun-Yeop Lee,
Pusan National University, Republic of Korea
Anne Cécile Grégoire,
ASNR - Autorité de Sûreté Nucléaire et de Radioprotection, France

*CORRESPONDENCE
Mariam,
mariamm@barc.gov.in

RECEIVED 25 March 2025
ACCEPTED 23 June 2025
PUBLISHED 05 August 2025

CITATION
Mariam, Joshi M, Nakhwa A, Khandare P, Soumen S, Khan A and Sapra BK (2025) Experimental insights into the formation and characterization of iodine oxide aerosols. *Front. Nucl. Eng.* 4:1599740. doi: 10.3389/fnuen.2025.1599740



# Experimental insights into the formation and characterization of iodine oxide aerosols

Mariam[1,2]*, Manish Joshi[1], Amruta Nakhwa[1], Pallavi Khandare[1], Samanta Soumen[1], Arshad Khan[1] and B. K. Sapra[1,2]

[1]Radiological Physics and Advisory Division, Bhabha Atomic Research Centre, Mumbai, India, [2]Homi Bhabha National Institute, Anushaktinagar, Mumbai, India

**Introduction:** A significant quantity of radioactive iodine is expected to be released following severe nuclear reactor accidents. Recent studies have shown that among various species expected, iodine oxides ($I_xO_y$) are less explored but play a crucial role in nuclear safety assessments due to their impact on source term evaluation. Therefore, this study was designed to generate and characterize iodine oxides in a laboratory scale setup.

**Methods:** Experiments were conducted at room temperature and ambient relative humidity using an $I_2$ concentration of ~1 ppm and an $O_3$ concentration of ~30 ppm inside a controlled chamber. The reaction kinetics were determined by continuously monitoring $O_3$ concentration. While many previous studies have relied on the radioactive iodine tracers and gamma spectroscopy, this study adopts an alternative approach by analysing ozone decay as a proxy for iodine oxidation. The generated iodine oxide aerosols were characterized for their physical and chemical properties. Impactors and gross samplers were used to collect aerosols, giving particle mass size distribution and total mass concentration, respectively. Particle morphology and chemical composition were determined using a scanning electron microscope (SEM), energy-dispersive X-ray spectroscopy (EDX), and X-ray photoelectron spectroscopy (XPS).

**Results and discussion:** The reaction kinetics showed that ozone decay followed first-order kinetics with a high correlation ($R^2 > 0.99$). The particles were found to have $I_2O_5$ chemical species with varied shapes, from small porous cloud-like structures to large rod-shaped particles. The findings provide valuable insights into iodine oxidation under environmentally relevant conditions, bridging knowledge gaps in source term estimation and contributing to the enhancement of accuracy of the modeling codes for nuclear safety applications.

KEYWORDS

**iodine oxides, source term, aerosols, chemical characterization, iodine oxidation**

## 1 Introduction

The release of radioactive materials following a Severe nuclear reactor accident, known as the source term, is crucial for public health risk assessment (Stewart et al., 2012; Lee et al., 2022). Among these, iodine is a major concern due to its volatility, environmental persistence, thyroid affinity, and complex chemistry. It exists in multiple oxidation states and chemical forms (aerosol, organic, and inorganic), influencing dose

coefficients essential for risk evaluation (Stewart et al., 2012). Historical reactor accidents such as Three Mile Island (1979), Chernobyl (1986), and Fukushima Daiichi (2011) have released significant amounts of radioactive iodine isotopes into the environment (Imanaka et al., 2015; Steinhauser et al., 2014). Initially, CsI was assumed to be the dominant iodine species entering containment, with minor contributions from other forms (Beahm et al., 1992; Soffer et al., 1995). However, later studies revealed that iodine speciation is more complex, influenced by reactor conditions, environmental factors, and radiolysis (Wren et al., 2000; Hou et al., 2013; Guentay et al., 2005). Phébus experiments further showed that iodine can be present in both gaseous and particulate forms with varied distribution depending on accident scenarios (Birchley et al., 2005; March et al., 2006; Jacquemain et al., 1999). For over 40 years, iodine behavior has been studied to improve source term predictions during severe nuclear accidents (Bosland and Jabet, 2024).

Recent studies show that air radiolysis products like ozone ($O_3$) and ionizing radiation oxidize iodine species to form iodine oxides, which nucleate into iodine oxide particles ($I_xO_y$) (Dickinson et al., 2014; Funke et al., 2012; Herranz et al., 2015; Kärkelä et al., 2010; Kärkelä et al., 2015). These oxides are involatile and may deposit on surfaces or dissolve in water (Dickinson et al., 2014). Radiolytic $I_2$ oxidation, which converts volatile iodine into aerosols, significantly influences its removal rate, making it key to source term assessments (Funke et al., 2012). Iodine oxides have been investigated by several international programs as well due to the crucial role in source term estimation and mitigation strategies. The PARIS program examined $I_2$ reactivity with air radiolysis products and aerosol kinetics (Bosland et al., 2008; Bosland et al., 2011). The THAI program (Funke et al., 2012) and the EXCSI facility at VTT, Finland (Kärkelä et al., 2009), explored iodine oxide aerosols formation from $I_2$ and $O_3$ reactions. The STEM project studied particulate $I_xO_y$ decomposition, identifying stable and unstable iodine oxides such as $I_2O_4$, $I_4O_9$, and $I_2O_5$ (Leroy and Bosland, 2023). Computational modeling studies designed to understand iodine oxides behavior in reactor accidents have also highlighted the role of iodine oxides in transport and deposition, challenging earlier models and improving radiological assessments (Dickinson et al., 2014; Lee and Cho, 2022; Bosland et al., 2010). Research on iodine oxides has focused on three key aspects: aerosol size, chemical composition, and radiolytic reaction rates. Aerosol size affects transport, deposition, and filtration efficiency, while chemical composition determines stability and reactivity. Reaction rate studies provide insights into iodine oxidation kinetics, crucial for accurate source term predictions. Together, these factors shape the understanding of iodine oxides behavior in nuclear accidents.

Aerosol size is a critical parameter for characterization, making the determination of iodine oxides aerosol size a key focus in numerous studies. For instance, THAI IOD 13 and 14 tests reported initial iodine oxide particle sizes of ~0.2 μm, increasing to ~0.4 μm due to agglomeration (Dickinson et al., 2014). In EXCSI, iodine oxides particle sizes ranged from tens to a few hundred nanometers (Ristovski et al., 2006). Uncertainties remain regarding the exact chemical composition, as iodine oxides may exist in multiple forms (Dickinson et al., 2014). The complex radiolytic reaction mechanism can be simplified into two steps: first, the formation of oxidizing agents, and second, the oxidation of gaseous $I_2$ into $I_xO_y$ aerosols by these agents (Funke et al., 1999; Bosland et al., 2008).

$$\text{air} + \text{Radiation} \longrightarrow O_3$$
$$I_2 / \text{Org I} + O_3 \longrightarrow I_xO_y$$

The third key aspect, radiolytic reaction rates, has been explored by several researchers. Funke (2000) studied the radiolytic decomposition for high $I_2$ concentrations, observing an initial zero-order reaction rate. This zero-order behavior suggests that the rate is constrained by the formation of a reactive species in the irradiated air/steam environment. In contrast, the PARIS program (Bosland et al., 2008; Bosland et al., 2011) examined radiolytic oxidation at lower initial $I_2$ concentrations, revealing decomposition kinetics that deviated from Funke's (2000) findings. The results indicated a shift toward first-order kinetics at lower $I_2$ concentrations, challenging the previously established zero-order assumption. Similarly, Tang and Castleman (1970) studied the radiolytic decomposition of gaseous $CH_3I$ in air, reporting zero-order kinetics at high concentrations but a transition to pseudo first-order kinetics within the relevant concentration range.

Despite advancements, knowledge gaps persist in $I_xO_y$ formation, transport, and impact, with oxidation kinetics under reactor accident conditions requiring further validation. Sinitsyn et al. (2024) highlighted that iodine oxides nanoparticle formation within containment can reduce filter efficiency, posing a long-term radiological hazard. Addressing these gaps through experimental studies is essential for improving nuclear accident response and iodine emission mitigation. Therefore, in this study, experiments were carried out to achieve radiolytic conversion of gaseous iodine ($I_2$) into $I_xO_y$ aerosols using $O_3$ and analyzing their physical and chemical characteristics. The experiments were carried out under ambient room conditions to complement previous studies, such as those conducted within the THAI program, which primarily focused on elevated conditions to simulate severe nuclear accident scenarios. In contrast, our aim was to investigate under typical laboratory or environmental conditions, which are more representative of initial release or ambient atmospheric processes. The research aims to determine the size distribution, morphology, and rate constant of the formed $I_xO_y$ particles, providing insights into their dynamics. Understanding these parameters is essential for refining iodine source term models, improving filtration and mitigation strategies, and enhancing nuclear safety protocols.

## 2 Materials and methods

The experiment was designed to convert gaseous iodine ($I_2$) into iodine oxides ($I_xO_y$) using $O_3$ inside a 0.2 $m^3$ perspex chamber (Figure 1). This chamber, equipped with multiple sampling lines, was placed inside a walk-in chamber to ensure workplace safety (Figure 2). The ozone generator, oxygen concentrator, and iodine chamber were positioned outside the walk-in chamber and connected to the perspex chamber via sampling lines. The chamber was flushed with clean air before the start of the experiment, and experiments were carried out under room

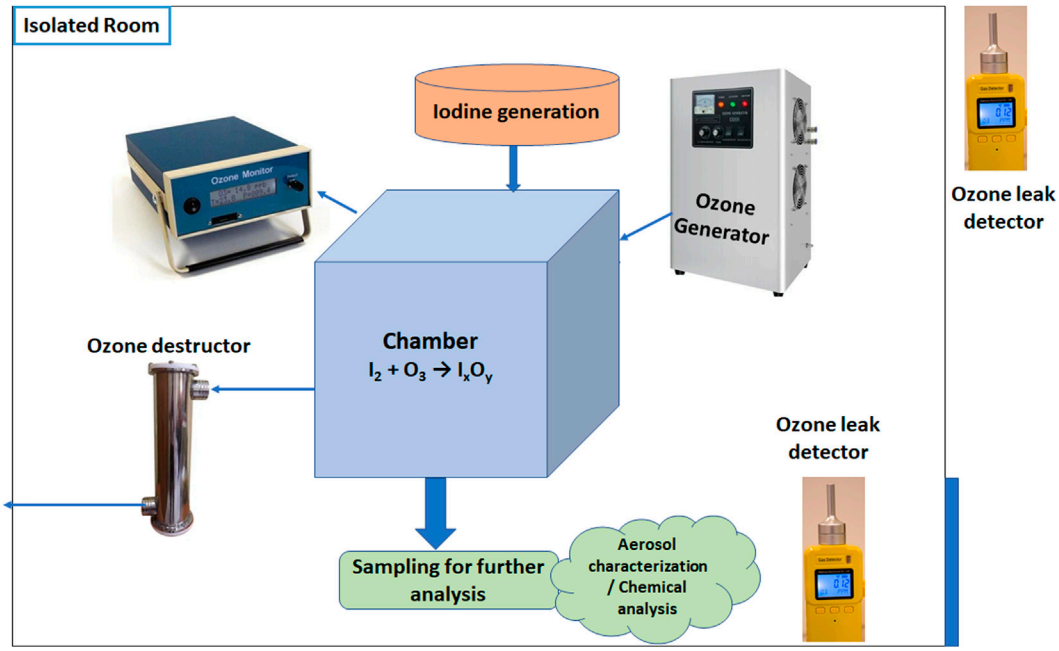


FIGURE 1
Schematic of experimental set-up.

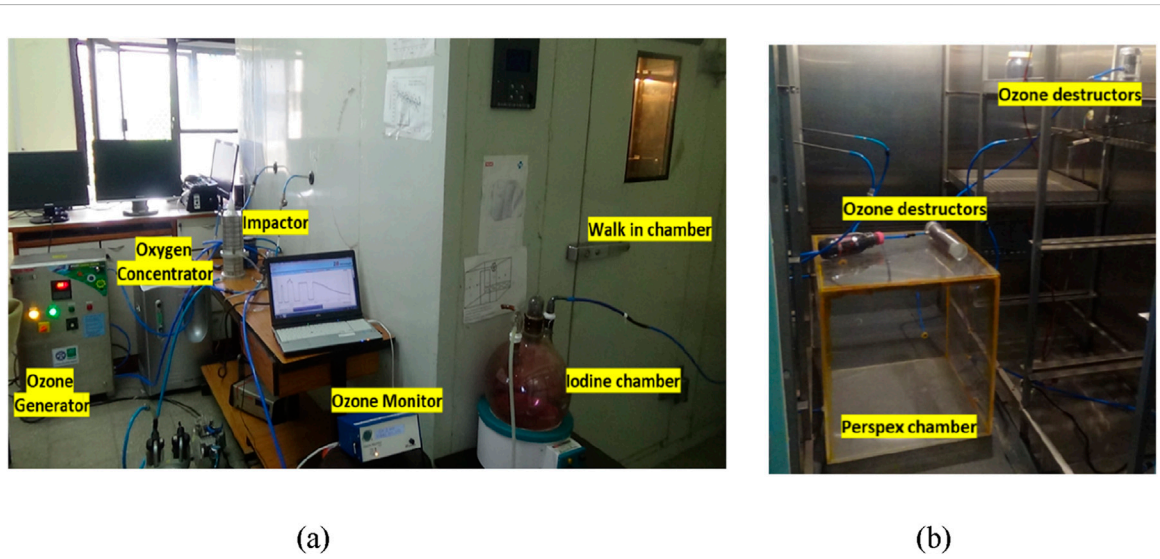


FIGURE 2
Picture of **(a)** experimental set-up and **(b)** inside of walk-in chamber.

conditions. The chamber environment was equilibrated with the outside ambient conditions, and no difference in temperature and relative humidity was noted in the sensors placed at both locations during scoping tests. Temperature and relative humidity characterizing the outside ambient environment were measured during the experiments and were found to remain within the range of 25°C–30°C and 50%–55%, respectively. Due to the possibility of iodine vapor deposition on sensors, we could not place any instruments in the chamber. In addition to that, the chamber was operated at atmospheric pressure only. A zero filter was attached to a port to maintain atmospheric pressure and balance pressure differences, if any.

$O_3$ was produced using an ozone generator (OZ-AIR ILG-OXY-WC, Nominal $O_3$ production ≥20 g/h) coupled with an oxygen concentrator (dry filtered oxygen with 90% outlet purity) and introduced into the perspex chamber. The $O_3$ concentration was continuously monitored using an ozone monitor (2B Technologies, 106-M) based on UV absorption (linear dynamic range: 0–1,000 ppm, resolution: 0.01 ppm), which provided real-time measurements to maintain controlled reaction conditions. Once a

steady-state $O_3$ concentration was achieved, the injection was stopped, and $I_2$ vapors generated by controlled heating were introduced using an external pump. The reaction progression was monitored using an ozone monitor instead of iodine because of the possibility of continuous and real-time measurement with the high resolution (1 Hz) of the former instrument. To minimize interference from iodine in UV-based ozone measurements at 254 nm, the sampling line to the ozone monitor was kept long and submerged in an ice bath. This setup allowed $I_2$ to condense before reaching the detector, ensuring accurate $O_3$ quantification.

The $I_2$ generation system consisted of a 10-L glass chamber, which was heated to approximately 100°C to facilitate the generation of $I_2$ vapor. Filtered air was pushed into the chamber at a flow rate of 5 LPM for 10 min, achieving more than 99% clearance. The $I_2$ concentration in the chamber was indirectly inferred from the amount of iodine pellets subjected to heating and the volume of the chamber. The direct quantification was not performed in each trial; however, a separate experiment (measurement of $I_2$ using UV–Vis spectroscopy) was carried out to validate this methodology.

Instruments for aerosol characterization and chemical analysis were connected to the chamber. This study used an Anderson low-pressure cascade impactor (Anderson, 0.1 μm–21 μm, flow rate: 10 LPM, pressure: 150 mmHg) based on inertial impaction to get size-segregated aerosol samples for particle size distribution analysis. A gross sampler with glass fiber filter paper was used to obtain total mass concentration by collecting bulk aerosols. The sampling flow rate and the duration were 10 LPM and 20 min, respectively. To characterize the aerosol products (iodine oxides) formed during the reaction, impactor and gross filter samplings were conducted at the end of the experiment. These sampling methods were employed to investigate particle size distribution, morphology, and chemical composition and were not intended to study the reaction kinetics. The kinetics of $O_3$ decay was monitored separately using continuous data from the ozone monitor throughout the experiment.

These aerosols collected on glass fiber filter papers were used for further chemical analysis. A scanning electron microscope (SEM) was used to obtain high-resolution imaging to analyze aerosol morphology and size, and energy-dispersive X-ray spectroscopy (EDX) was used to identify and quantify the elemental composition of iodine oxide particles. Additionally, X-ray photoelectron spectroscopy (XPS) was used to determine the oxidation states of iodine within the collected aerosols, providing insights into their chemical composition.

All experiments were carried out in a static condition; that is, after inserting the $I_2$ and $O_3$, the ports were closed to allow unperturbed reaction progression. To prevent any environmental or health hazards from the $O_3$, the exhaust of the sampling pump was connected to an ozone destructor unit. To summarize, the experiment can be subdivided into three phases:

1) $I_2$ Injection Phase: The iodine chamber (10 L) was flushed with air at 5 LPM for 10 min. Based on the calculated clearance time (9 min for 99% clearance at 30 ACH), the injection phase ensured complete transfer of iodine vapor into the main reaction chamber.
2) Reaction Phase and $O_3$ Monitoring: The $O_3$ decay kinetics study began immediately after phase 1, i.e., after the completion of iodine injection.
3) Sampling Phase: Approximately 10 min were allowed for completion of gas-to-particle conversion (sufficient for the depletion of one of the reactants, viz., $O_3$, to background levels). Gross filter sampling (20 LPM for 10 min) and impactor sampling (10 LPM for 20 min) were initiated after 10 min. The objective of the sampling was to characterize the physical and chemical properties of the aerosol.

# 3 Results and discussions

Two sets of experiments were conducted to study the $O_3$ decay kinetics and the characteristics of $I_xO_y$ aerosols. Initially, the chamber contained $O_3$ and $I_2$ concentrations of approximately 30 ppm and ~1 ppm, respectively, resulting in an ozone-to-iodine ratio of 30:1. The high ratio ensured the complete conversion to iodine oxides. The methodology is consistent with other studies, such as the THAI experiments. Maintaining a high $O_3$ concentration relative to $I_2$ is crucial as it promotes efficient oxidation and facilitates the formation of iodine oxide aerosols. The first confirmation of the conversion of iodine vapor to $I_xO_y$ aerosols came from the collection of aerosols on a gross sampler. Experimental observations confirmed the rapid formation of iodine oxides through the oxidation of molecular iodine at room temperature. The obtained mass concentrations on the gross sampler were ~20 mg/m$^3$.

## 3.1 Aerosol size characterization

Numerous studies have shown that the radiolytic decomposition of $I_2$ and $CH_3I$ leads to the formation of fine $I_xO_y$ aerosols with diameters below 1 μm (Funke et al., 2012; R'mili et al., 2022). However, study by Leroy and Bosland (2023) revealed the presence of $I_xO_y$ particles with a broad size distribution with three size ranges: the largest (>5 μm) accounted for 20%, while the intermediate (2–5 μm) and smallest (<1 μm) constituted the remaining 80%. In this study, aerosol size was characterized by using an impactor and SEM images. Figure 3 shows the mass size distribution obtained by the impactor. Each stage of the impactor was analyzed gravimetrically, and the filters were pre-conditioned in the desiccator prior to the sampling. The analysis shows that 70% of the formed particles lie between 1.13 μm and 2.23 μm. This is similar to the observation of the study by Leroy and Bosland (2023), where only ~10% of the particles were >5 μm. Most of the particles (80%) lay in the range of 1–5 μm. This similarity may be attributed to the similar way of generation (excess of $O_3$ relative to $I_2$, low concentrations, and static chamber). These submicron aerosols may thereafter serve as nucleation sites, promoting the growth of larger iodine oxides aggregates.

The SEM analysis was conducted at an accelerating voltage of 15 kV with a working distance of approximately 10 mm. The images were captured using a secondary electron detector at a resolution suitable for surface morphological characterization, approximately 3–5 nm. Prior to SEM observation, the samples were sputter-coated

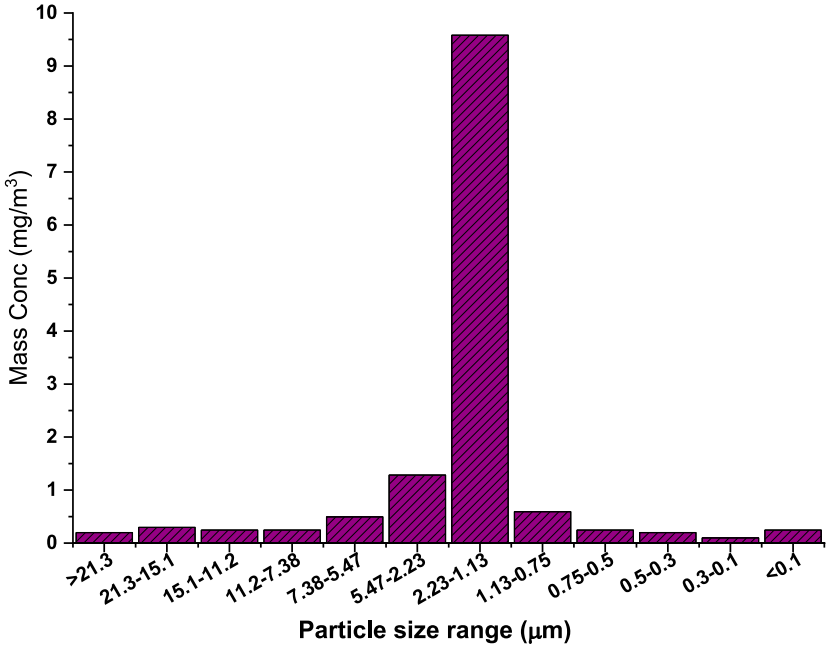


FIGURE 3
Mass size distribution of $I_xO_y$ particles obtained from the impactor.

with a thin (~10 nm) layer of gold to minimize surface charging effects and improve imaging quality. Gold was chosen due to its excellent conductivity and compatibility with SEM-EDX analysis, without interfering with the detection of key elements such as iodine or oxygen. SEM images (Figure 4) reveal $I_xO_y$ aerosols exhibiting both rod-like and fluffy cloud-like structures, indicating diverse morphologies. This morphological diversity aligns with findings from previous studies, which have shown that $I_xO_y$ particles can form fractal-like aggregates with varying shapes and sizes, influenced by factors such as relative humidity and the specific iodine oxide species present (R'Mili et al., 2022; Saunders and Plane, 2006). Funke et al. (2012) reported that particles undergo growth via agglomeration, leading to larger, more irregular formations over time. The presence of both rod-like and cloud-like structures in the present study is consistent with previous findings, where iodine oxide aerosols display heterogeneous morphology due to differing nucleation and growth mechanisms.

## 3.2 Chemical characterization

Several studies have investigated the chemical composition of $I_xO_y$, identifying potential oxidation products such as $I_2O_4$, $I_2O_5$, $I_4O_9$, and $HIO_3$ (Kärkelä et al., 2009; Glowa and Ball, 2012). Research suggests that $I_2O_4$ plays a pivotal role in the early polymerization steps leading to $I_xO_y$ formation (Martín et al., 2013; Ristovski et al., 2006; Tietze et al., 2012; Saunders et al., 2010). Successive oxidation of primary species (I, IO, $IO_2$) in the presence of $O_3$ ultimately produces $I_4O_9$, while $I_2O_4$ and its dimer are thought to undergo polymerization, initiating aerosol nucleation (Martín et al., 2013). The IODAIR model (Dickinson, 1998) suggests that radiolytic $I_2$ oxidation is primarily driven by reactions with OH, O, and H radicals, forming intermediates such as HOI, HI, IO, $INO_2$, and $IONO_2$. A key precursor, $IO_2$, arises through a minor pathway involving $O_3$ reactions with $I_2$ or IO, subsequently dimerizing into $I_2O_4$ and other oxides (Dickinson et al., 2014).

1) $IO_2+IO_3 \longrightarrow I_2O_4$
2) $I_2O_4+IO_2 \longrightarrow I_3O_6$
3) $I_3O_6+IO_2 \longrightarrow I_2O_8$
4) $I_2O_8+O_3 \longrightarrow I_4O_9I$

However, Sipil¨a et al. (2016) proposed an alternative mechanism in which aerosols form via sequential addition of $HIO_3$, followed by intra-cluster restructuring to $I_2O_5$ and water recycling through dehydration. In chamber studies of the $I_2$ with hν and $O_3$ system, Saunders and Plane (2006) suggested that $I_2O_5$ was more likely to be formed through successive oxidation of $I_2O_2$, $I_2O_3$, and $I_2O_4$ in the presence of $O_3$. The reactive processes and composition of polymerizing iodine oxides remain uncertain, with intermediate reactions leading to aerosol formation still poorly understood (Kumar et al., 2018; Martín et al., 2020).

1) $I_2O_2+O_3 \longrightarrow I_2O_3$
2) $I_2O_3+O_3 \longrightarrow I_2O_4$
3) $I_2O_4+O_3 \longrightarrow I_2O_5$
4) $I_2O_5 + (I_2O_5)_n \longrightarrow (I_2O_5)_{n+5}$

To address the uncertainty in the chemical composition of the formed $I_xO_y$, both EDX and XPS analyses were performed on aerosol samples collected using the gross sampler. Elemental mapping via EDX (Figure 5) confirmed the spatial distribution of iodine, indicating its presence within the observed structures. EDX, alongside SEM, enables qualitative elemental analysis by detecting

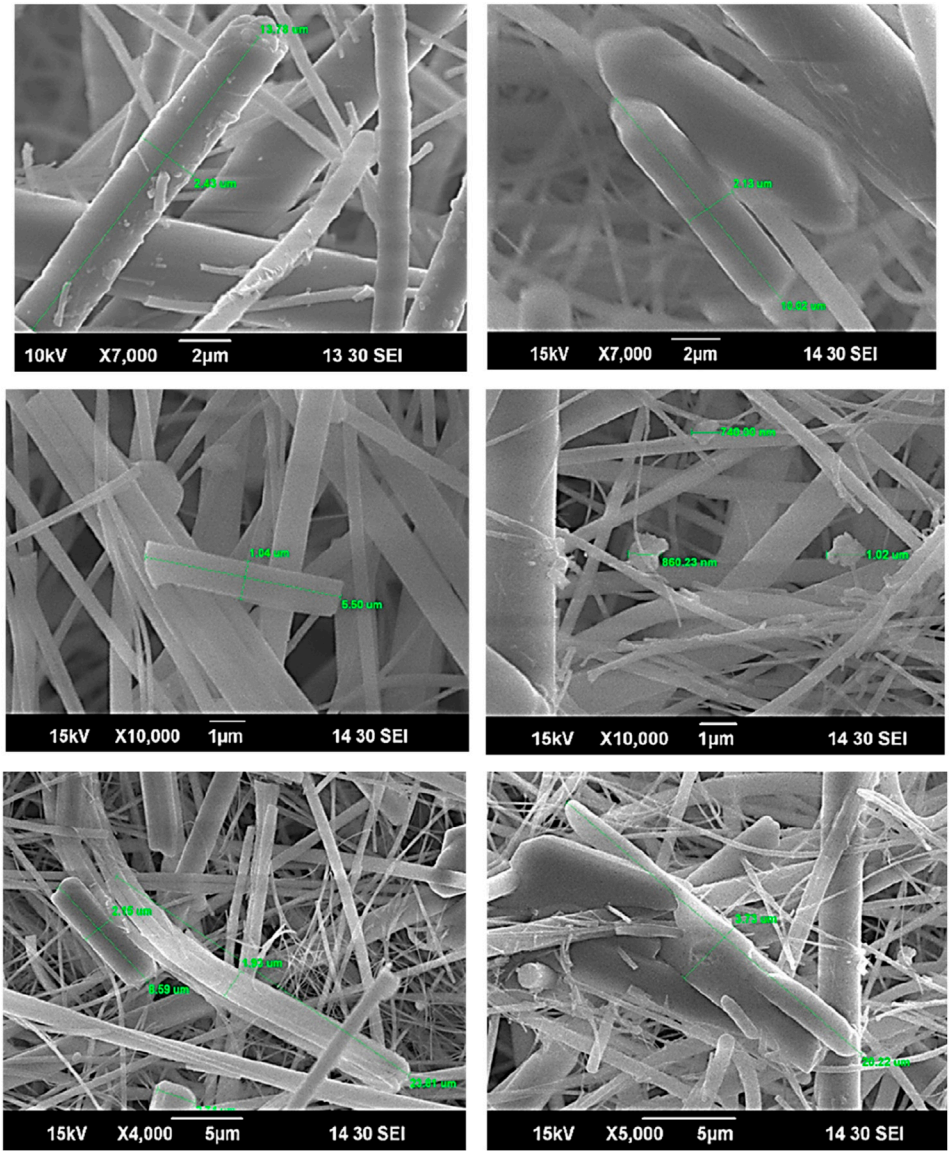


FIGURE 4
SEM images of $I_xO_y$ samples collected on glass fiber filter paper.

characteristic X-rays emitted upon electron beam interaction. Figure 6 shows the EDX spectra of the collected aerosol particles during experiments. The spectra exhibit prominent peaks corresponding to iodine and oxygen, thereby supporting the formation of iodine oxides.

To further determine the chemical composition of the iodine oxides, X-ray photoelectron spectroscopy (XPS) analysis was conducted, which confirmed the presence of $I_2O_5$. XPS is a powerful technique used to analyze the chemical composition and oxidation states of elements in a material by measuring the binding energy of emitted electrons upon X-ray irradiation. X-ray photoelectron spectroscopy (XPS) measurements were carried out using a DESA-150 electron analyzer (Staib Instruments, Germany) with a resolution of 2 eV, a pass energy of 40 eV, and Mg-Ka (1,253.6 eV) source. The accelerating voltage was 15 KeV, and the beam current was 15 mA. The binding energy was calibrated using an Au-4f7/2 line with an energy of 84.0 eV and a C-1s line with an energy of 284.8 eV. The deconvolution of high-resolution peaks was carried out using XPSPEAK4.1 software. The base pressure of the chamber was maintained at ~ $2 \times 10^{-8}$ mbar during the measurements. No additional surface coating was applied to XPS samples as the system includes a low-energy electron flood gun to neutralize surface charge during analysis.

In the case of $I_xO_y$, XPS can distinguish between different iodine oxidation states and identify specific iodine oxide compounds. The collected aerosol sample was first subjected to an XPS survey scan covering all binding energy ranges to detect elemental constituents (Figure 7a), giving a strong peak at I 3d. Further analysis of the I 3d region (Figure 7b) revealed two distinct peaks at binding energy positions of 623.5 eV and 634.96 eV, corresponding to iodine oxidation states indicative of $I_2O_5$ (Chastaine and King, 1995; Sherwood, 1976). In XPS analysis, the I 3d spectrum typically

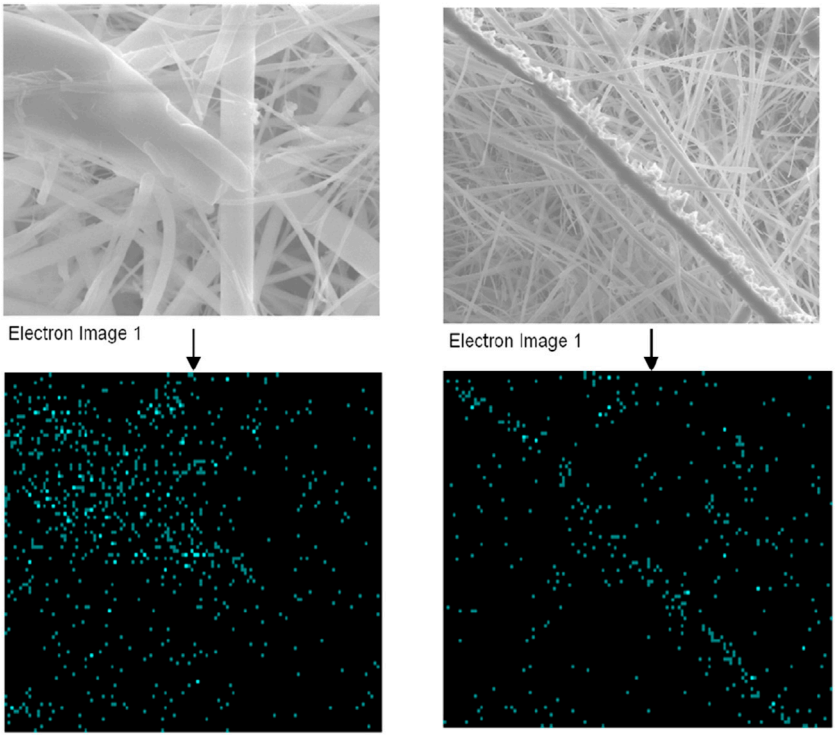


FIGURE 5
SEM images and EDX elemental mapping showing presence of iodine (cyan color dots represent iodine) (15 keV accelerating voltage and 10 mm working distance).

exhibits a doublet structure due to spin-orbit splitting, a common phenomenon in elements with relatively high atomic numbers. This splitting arises because the total angular momentum (J) of the electrons in the I 3d orbital can take two different values, leading to two distinct peaks. Table 1 provides detailed information on the peak positions, full width at half maximum (FWHM), and peak areas, further supporting the identification of $I_2O_5$ in the aerosol samples. Differences in experimental parameters, including reactant molar ratios, initial species concentrations, temperature, and relative humidity, can significantly influence the oxidation pathway and govern the speciation of the resulting iodine oxides. In this study, the aerosols were collected under oxidizing conditions with excess $O_3$, which facilitated the further oxidation of lower iodine oxides to $I_2O_5$.

## 3.3 Decay rate

Previous studies have primarily utilized tracer iodine species, using gamma spectroscopy to track iodine concentration and reaction kinetics (Funke et al., 2012; Dickinson et al., 2014). However, handling radioactive iodine was not feasible in our study, making direct monitoring of iodine decay impractical. As an alternative approach, we used the decay rate of $O_3$ for $I_2$ consumption, given that $O_3$ is the primary oxidizing agent in the reaction. Continuous monitoring of $O_3$ concentration using an ozone analyzer was carried out, and its decay rate was measured over time to infer the progress of iodine oxidation. This method provides an indirect yet effective way to assess $I_xO_y$ formation while ensuring safety and feasibility in a non-radioactive experimental setup.

Figures 8a,b show the decay of $O_3$ concentration following the introduction of $I_2$ into the chamber. By plotting $O_3$ concentration against time, the reaction rate constant and half-life were determined, following first-order exponential decay kinetics. The decay was modeled using a mono-exponential (ExeDec1, Equation 1) function:

$$y = Ae^{-\frac{x}{t}} + y_o \tag{1}$$

where y represents $O_3$ concentration (ppm), $y_o$ is residual or background ozone level when $t$ approaches ∞. x is time (s), and k is the rate constant ($s^{-1}$), which is the reciprocal of t. The half-life was calculated as (Equation 2)

$$t_{1/2} = \frac{0.693}{k} \tag{2}$$

The $O_3$ decay exhibited an excellent fit to first-order kinetics, as indicated by the high correlation coefficient ($R^2$ = 0.996). Additionally, plotting ln[A] vs. time yielded a linear fit ($R^2$ = 0.995), further confirming first-order reaction behavior (Figures 8c,d). The decay constants obtained for Set 1 and Set 2 were $8.3 \times 10^{-3}$ $s^{-1}$ and $5.2 \times 10^{-3}$ $s^{-1}$, respectively, with corresponding half-lives of 83.5 s and 133.3 s, showing good reproducibility.

To assess background $O_3$ decay in the absence of $I_2$, control experiments were conducted by inserting $O_3$ without $I_2$. The results

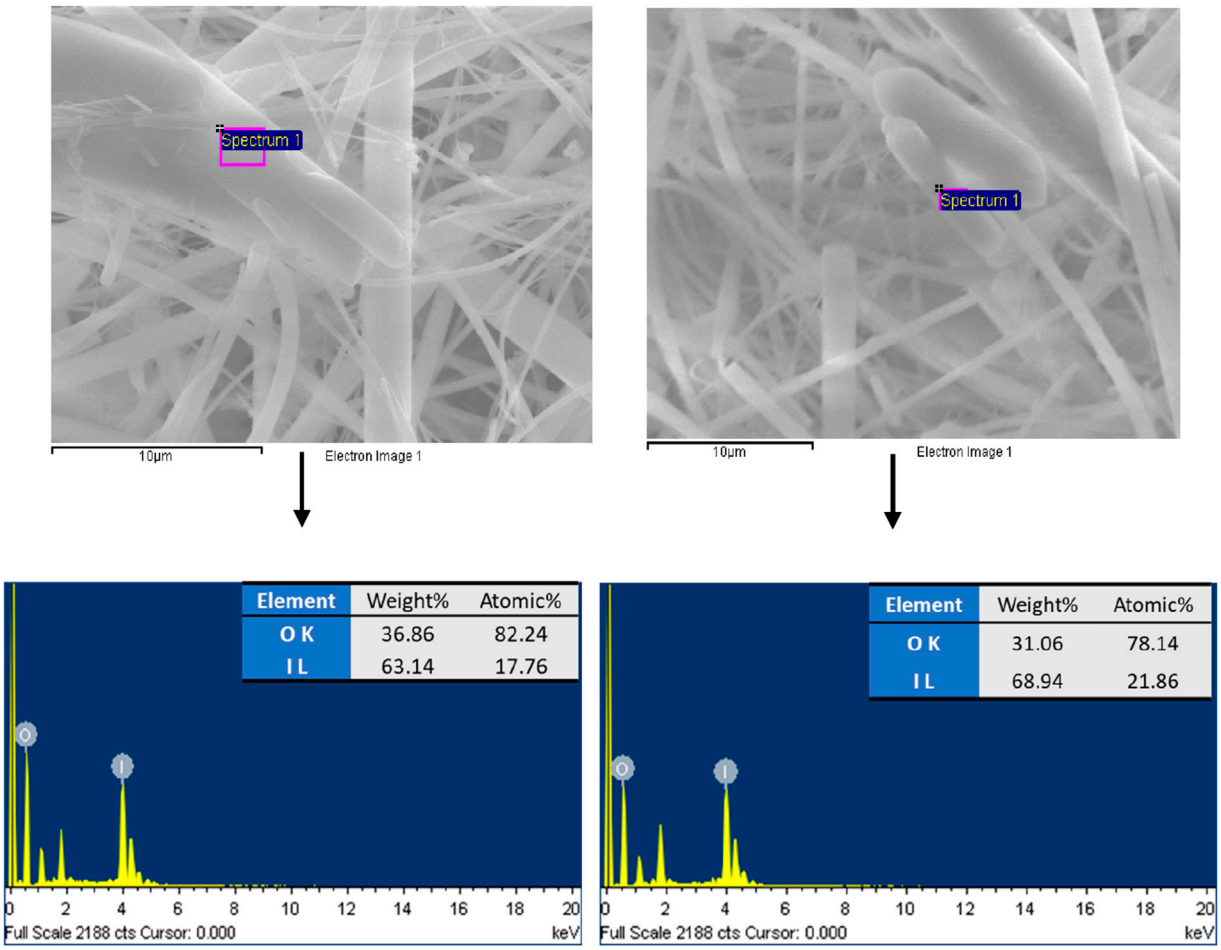


FIGURE 6
EDX elemental analysis of iodine oxides aerosol (corresponding to area in box, top).

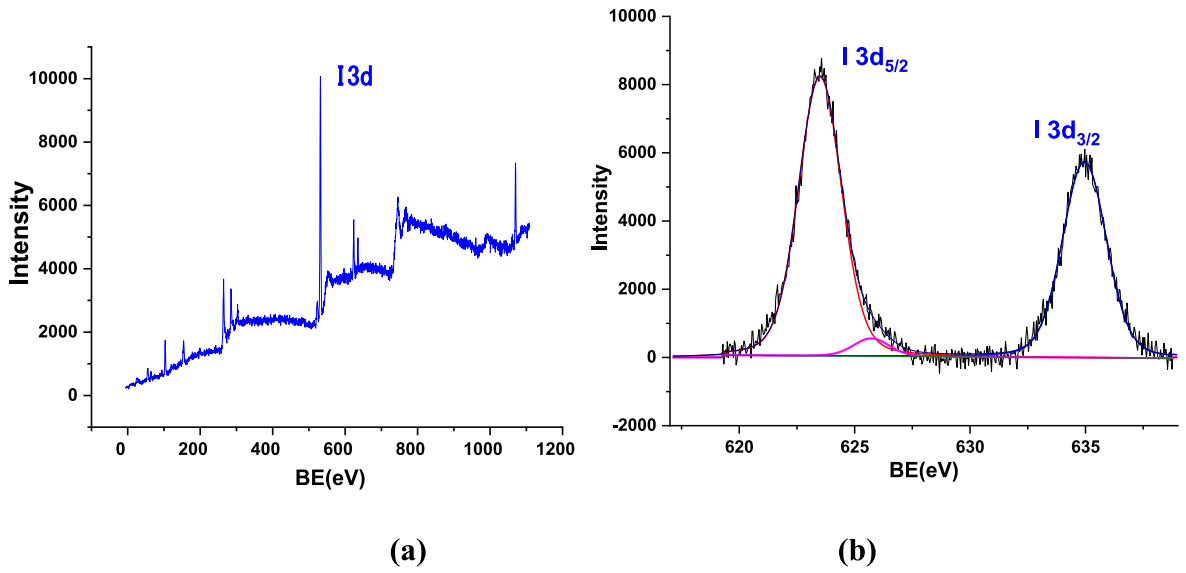


FIGURE 7
**(a)** XPS survey scan for all binding energies and **(b)** I 3d XPS spectra.

TABLE 1 Peak analysis of XPS for the iodine oxide sample.

| | Peak 1 | Peak 2 |
|---|---|---|
| Position | 623.5 | 634.96 |
| FWHM | 2.2 | 2.25 |
| Area | 20,741.17 | 14,903.38 |

showed negligible $O_3$ depletion, confirming that observed $O_3$ decay during actual experiments can be attributed to iodine chemistry. Figure 9 compares the decay of $O_3$ concentration with and without $I_2$.

The use of mono-exponential decay functions (Equation 1) for kinetic analysis is well-established in the literature (Mishra et al., 2013; Vicari et al., 2021; Smulders and Nitschke, 2012; Tsai et al., 2008; Remy et al., 2015). For instance, Smulders and Nitschke (2012) employed a similar approach to study the Diels–Alder reaction between furan and maleimide, where furan consumption was modeled using a mono-exponential decay function, and the reaction rate constant was determined.

In chemical kinetics, a first-order reaction is characterized by a rate directly proportional to the concentration of a single reactant, expressed as:

$$\text{Rate} = k[A]$$

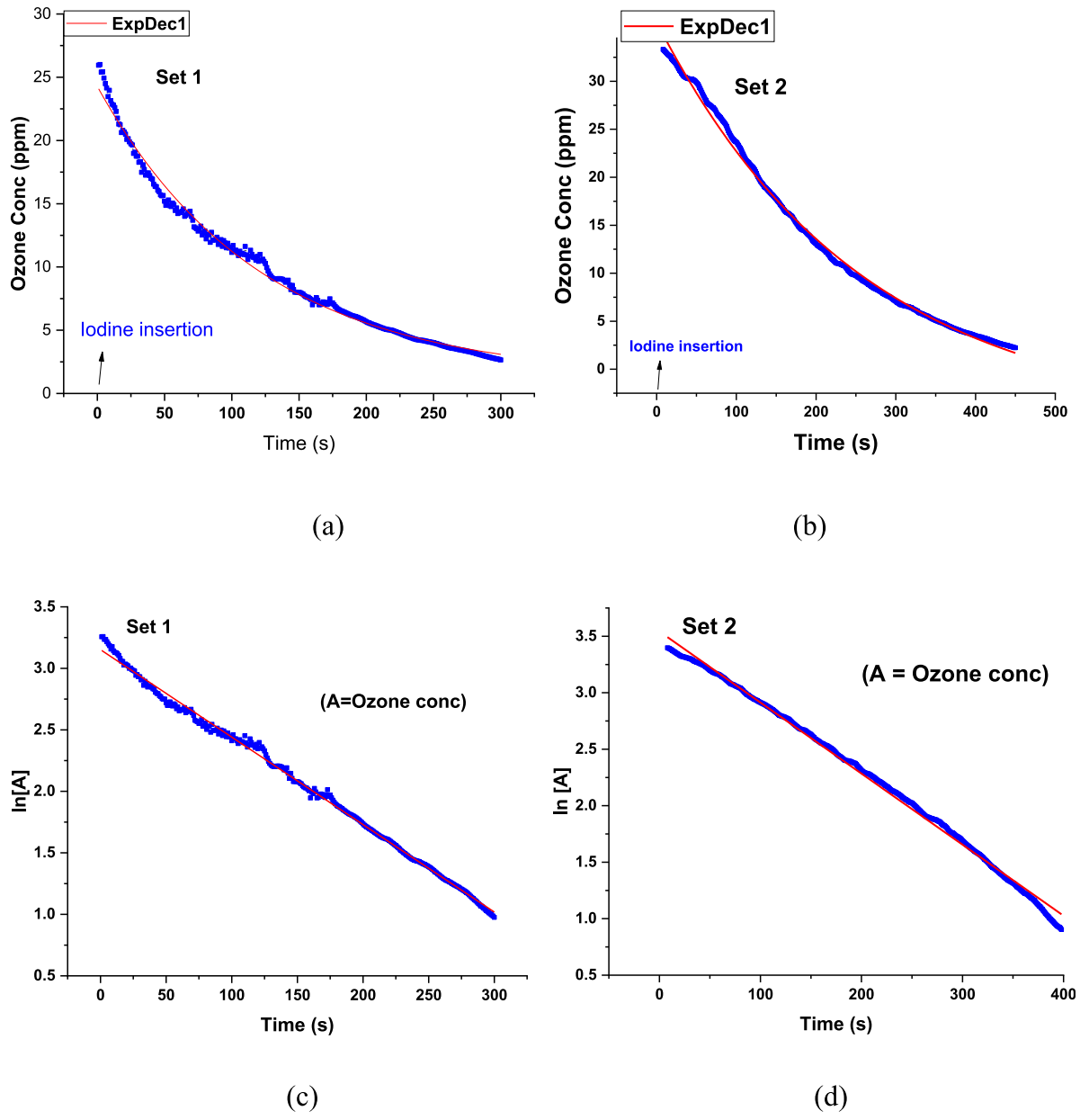


FIGURE 8
**(a,b)** Ozone concentration vs. time plot and **(c,d)** Ln [A] vs. time plot of Set 1 and Set 2 (The line-of-best-fit is shown in red.).

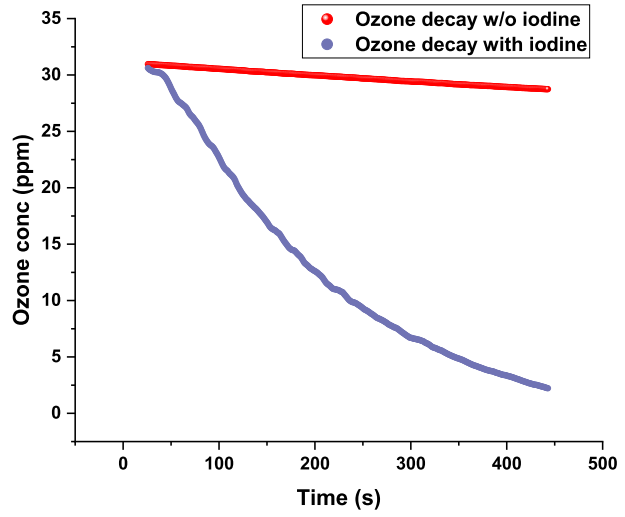


FIGURE 9
Ozone concentration vs. time plot: with and without iodine.

where k is the rate constant, and [A] is the reactant concentration. In a pseudo first-order reaction, a multi-reactant system behaves as if it follows first-order kinetics due to the presence of one reactant in large excess. The concentration of the excess reactant remains nearly constant throughout the reaction, allowing the rate law to be simplified to depend only on the limiting reactant.

Regarding the reaction between iodine ($I_2$) and ozone ($O_3$), studies have shown that the kinetics can exhibit first-order behavior under certain conditions. Funke (2000) observed zero-order kinetics for high $I_2$ concentrations, while the PARIS program (Bosland et al., 2008; Bosland et al., 2011) found a shift to first order at lower concentrations. Tang and Castleman (1970) reported a similar transition for $CH_3I$. The observed first-order ozone decay suggests that the reaction rate is primarily governed by ozone concentration, which could be due to the $O_3$-limited reaction or rapid iodine oxidation. If iodine is present in excess or reacts rapidly with ozone, then ozone concentration dictates the rate-determining step. This scenario is common in ozone-involved reactions, where ozone decay follows first-order kinetics. Otherwise, if the iodine oxidation step is fast relative to ozone decomposition, the reaction appears first-order with respect to ozone. While the reaction indicates first-order behavior with respect to ozone, further studies such as varying initial iodine concentrations or conducting detailed mechanistic analyses are necessary to confirm whether this is a true first-order reaction or a pseudo-first-order approximation. Unlike previous studies that relied on radioactive tracer iodine and gamma spectroscopy, the present study employs ozone decay as a proxy for iodine oxidation, allowing safe and continuous reaction monitoring without the complexities of handling radioactive iodine. This study bridges the data gap that can help in refining source term assessments and advancing computational modeling. The findings contribute to a better understanding of iodine oxides formation kinetics, providing valuable insights for nuclear safety and mitigation strategies in iodine-related environmental scenarios.

## 4 Conclusion

This study provides critical insights into the formation and characteristics of iodine oxides ($I_xO_y$) through the oxidation of molecular iodine ($I_2$) by ozone ($O_3$) under room conditions. One of the key distinctions of this study lies in its experimental conditions. While earlier studies, such as those conducted in large-scale facilities like THAI, explored iodine chemistry under extreme conditions (e.g., elevated temperatures and humidity levels), this research focuses on iodine oxidation in a more simplified yet environmentally relevant setting.

With an initial $I_2$ concentration of 1 ppm and $O_3$ at 30 ppm, the study demonstrated rapid $I_xO_y$ formation, confirming that iodine oxidation can proceed efficiently under ambient conditions. The study effectively demonstrates that iodine oxides can form rapidly under ambient conditions. High-resolution characterization techniques such as SEM, EDX, XPS, and impactor-based sampling provided a detailed analysis of the size, morphology, and elemental composition of $I_xO_y$ aerosols. The SEM images revealed both rod-like and cloud-like structures, indicating a complex aerosol formation process, while EDX and XPS confirmed the presence of iodine oxides, $I_2O_5$. Kinetic analysis showed first-order ozone decay, indicating ozone-limited reaction dynamics.

Understanding $I_xO_y$ formation at room temperature and relative humidity helps refine models related to aerosol nucleation, transport, and deposition, particularly in nuclear accident scenarios. By refining kinetic models and exploring broader reaction conditions, future research can enhance our understanding of $I_xO_y$ behavior in nuclear accident scenarios, ultimately improving risk assessment and mitigation strategies. This study uses ozone decay kinetics for determining iodine oxidation, enabling safe and continuous reaction monitoring without relying on radioactive tracers or gamma spectroscopy. In summary, this study not only reinforces the rapid oxidation of iodine by ozone under ambient conditions but also offers a methodological approach, detailed aerosol characterization, and robust kinetic analysis that distinguish it from previous research in the field.

## Data availability statement

The original contributions presented in the study are included in the article/supplementary material; further inquiries can be directed to the corresponding author.

## Author contributions

Mariam: Formal Analysis, Visualization, Methodology, Writing – original draft, Data curation, Investigation. MJ: Conceptualization, Writing – review and editing, Methodology, Investigation, Supervision. AN: Writing – original draft, Formal

Analysis, Visualization, Data curation. PK: Methodology, Writing – original draft, Formal Analysis, Data curation. SS: Resources, Writing – review and editing, Data curation, Formal Analysis. AK: Writing – review and editing, Conceptualization, Methodology, Supervision, Investigation. BS: Supervision, Conceptualization, Writing – review and editing, Project administration, Methodology.

## Funding

The author(s) declare that no financial support was received for the research and/or publication of this article.

## Acknowledgments

The authors sincerely thank Prof R.P. Chauhan, Department of Physics, National Institute of Technology, Kurukshetra, India, for providing the SEM facility for the analysis.

## Conflict of interest

The authors declare that the research was conducted in the absence of any commercial or financial relationships that could be construed as a potential conflict of interest.

## Generative AI statement

The author(s) declare that no Generative AI was used in the creation of this manuscript.

## Publisher's note



## References

Beahm, E. C., Weber, C. F., Kress, T. S., and Parker, G. W. (1992). *Iodine chemical forms in LWR severe accidents*. Washington, DC: Nuclear Regulatory Commission.

Birchley, J., Haste, T., Bruchertseifer, H., Cripps, R., Guntay, S., and Jackel, B. (2005). Phebus-FP: results and significance for plant safety in Switzerland. *Nucl. Eng. Des.* 235 (15), 1607–1633. doi:10.1016/j.nucengdes.2005.02.018

Bosland, L., Cantrel, L., Girault, N., and Clement, B. (2010). Modeling of iodine radiochemistry in the ASTEC severe accident code: description and application to FPT-2 Phebus test. *Nucl. Technol.* 171 (1), 88–107. doi:10.13182/nt10-a10774

Bosland, L., Funke, F., Girault, N., and Langrock, G. (2008). PARIS project: radiolytic oxidation of molecular iodine in containment during a nuclear reactor severe accident. *Nucl. Eng. Des.* 238 (12), 3542–3550. doi:10.1016/j.nucengdes.2008.06.023

Bosland, L., Funke, F., Girault, N., and Langrock, G. (2011). PARIS project: radiolytic oxidation of molecular iodine in containment during a nuclear reactor severe accident: Part 2: formation and destruction of iodine oxides compounds under irradiation –experimental results modelling. *Nucl. Eng. Des.* 241 (9), 4026–4044. doi:10.1016/j.nucengdes.2011.06.015

Bosland, L., and Jabet, K. C. (2024). Main lessons learnt from 40 years of R&D on iodine source term prediction: identification of the main parameters governing iodine volatility in PHEBUS FP tests. *Prog. Nucl. Energy* 177, 105473. doi:10.1016/j.pnucene.2024.105473

Chastain, J., and King Jr., R. C. (1995). *Handbook of X-ray photoelectron spectroscopy, physical electronics, eden prairie*.

Dickinson, S. (1998). ICHEMM final synthesis report. *5th EURATOM Framew. PROGRAMME (1998–2002) SAM–ICHEMM–D021*. Available online at: cordis.europa.eu/documents/documentlibrary/66627231EN6.pdf (Accessed January, 2014).

Dickinson, S., Auvinen, A., Ammar, Y., Bosland, L., Clement, B., Funke, F., et al. (2014). Experimental and modelling studies of iodine oxide formation and aerosol behaviour relevant to nuclear reactor accidents. *Ann. Nucl. Energy* 74, 200–207. doi:10.1016/j.anucene.2014.05.012

Funke, F. (2000). *Literature review on the radiolytic oxidation of molecular iodine in the containment atmosphere*. EC. Report SAM-ICHEMM-D002.

Funke, F., Langrock, G., Kanzleiter, T., Poss, G., Fischer, K., Kühnel, A., et al. (2012). Iodine oxides in large-scale Thai tests. *Nucl. Eng. Des.* 245, 206–222. doi:10.1016/j.nucengdes.2012.01.005

Funke, F., Zeh, P., and Hellmann, S. (1999). *Radiolytic oxidation of molecular iodine in the containment atmosphere, OECD Workshop on iodine aspects of severe accident management*. Finland: Vantaa, 18–20.

Glowa, G. A., and Ball, J. M. (2012). *Gas phase radiolysis of iodine*. Report No.: 153-126530-440-017. Atomic Energy of Canada Limited.

Guentay, S., Cripps, R. C., Jäckel, B., and Bruchertseifer, H. (2005). Iodine behaviour during a severe accident in a nuclear power plant. *CHIMIA* 59 (12), 957. doi:10.2533/000942905777675453

Herranz, L. E., Haste, T., and K¨arkel¨a, T. (2015). Recent advances in the source term area within the SARNET European severe accident research network. *Nucl. Eng. Des.* 288, 56–74. doi:10.1016/j.nucengdes.2015.03.014

Hou, X., Pavel, P., Zhang, L., Shi, K., Biddulph, D., Chang, C. C., et al. (2013). Iodine-129 in seawater offshore Fukushima: distribution, inorganic speciation, sources, and budget. *Environ. Sci. and Technol.* 47 (7), 3091–3098. doi:10.1021/es304460k

Imanaka, T., Hayashi, G., and Endo, S. (2015). Comparison of the accident process, radioactivity release and ground contamination between Chernobyl and Fukushima-1. *J. Radiat. Res.* 56, i56–i61. doi:10.1093/jrr/rrv074

Jacquemain, D., Hanniet, N., Poletiko, C., Dickinson, S., Wren, C., Powers, D., et al. (1999). An overview of the iodine behaviour in the two first PHEBUS tests FPT-0 and FPT-1, OECD Workshop on iodine aspects of severe accident management. Vantaa, Finland, May 18–20.

Kärkelä, T., Auvinen, A., Kekki, T., Kotiluoto, P., Lyyränen, J., and Jokiniemi, J. (2015). Radiolytical oxidation of gaseous iodine by beta radiation. *Radiochim. Acta.* 103 (10), 719–728. doi:10.1515/ract-2015-2417

Kärkelä, T., Holm, J., Auvinen, A., Ekberg, C., Glänneskog, H., Tapper, U., et al. (2009). "Gas phase oxidation of elemental iodine in containment conditions," in ICONE17: Proceedings of the 17th International Conference on Nuclear Engineering (New York: ASME).

Kärkelä, T., Holm, J., Auvinen, A., Zilliacus, R., Kajolinna, T., Tapper, U., et al. (2010). "Gas phase reactions of organic iodine in containment conditions," in ICAPP2010: Proceedings of the International Congress on Advances in Nuclear Power Plants 2010 (New York: Curran Associates).

Kumar, M., Saiz-Lopez, A., and Francisco, J. S. (2018). Single-molecule catalysis revealed: elucidating the mechanistic framework for the formation and growth of atmospheric iodine oxide aerosols in gas-phase and aqueous surface environments. *J. Am. Chem. Soc.* 140 (44), 14704–14716. doi:10.1021/jacs.8b07441

Lee, Y., and Cho, Y. J. (2022). Analyses on importance of iodine chemistry models in AnCheBi code for a severe accident of nuclear power plant. *Ann. Nucl. Energy* 171, 109021. doi:10.1016/j.anucene.2022.109021

Lee, Y., Jin, Y., and Lim, K. (2022). Numerical studies on the important fission products for estimating the source term during a severe accident. *Nucl. Eng. Technol.* 54 (7), 2690–2701. doi:10.1016/j.net.2022.02.025

Leroy, O., and Bosland, L. (2023). Study of the stability of iodine oxides (IxOy) aerosols in severe accident conditions. *Ann. Nucl. Energy* 181 (181109526), 109526. doi:10.1016/j.anucene.2022.109526

March, P., Biard, B., Manenc, C., Payot, F., Gaillard, C., Guillot, J., et al. (2006). "First results of the PHEBUS FPT3 test," in 14th International Conference onNuclear Engineering, Miami, Florida, USA, July 17-20, 205–214. doi:10.1115/icone14-89432

Martín, J. C. G., G´alvez, O., Baeza-Romero, M. T., Ingham, T., Plane, J. M. C., and Blitz, M. A. (2013). On the mechanism of iodine oxide particle formation. *Phys. Chem. Chem. Phys.* 15 (37), 15612–15622. doi:10.1039/c3cp51217g

Martín, J. C. G., Lewis, T. R., Blitz, M. A., Plane, J. M., Kumar, M., Francisco, J. S., et al. (2020). A gas-to-particle conversion mechanism helps to explain atmospheric particle formation through clustering of iodine oxides. *Nat. Commun.* 11 (1), 1–14. doi:10.1038/s41467-020-18252-8

Mishra, S., Anand, D., Vijayarangan, N., and Ajitkumar, P. (2013). An accurate method for the qualitative detection and quantification of mycobacterial promoter activity. *Open Microbiol.* 7, 1–5. doi:10.2174/1874285801307010001

Remy, P.-Ph., Etique, M., Hazotte, A. A., Sergent, A. S., Estrade, N., Cloquet, C., et al. (2015). Pseudo-first-order reaction of chemically and biologically formed green rusts with HgII and C15H15N3O2: effects of pH and stabilizing agents (phosphate, silicate, polyacrylic acid, and bacterial cells). *Water Res.* 70, 266–278. doi:10.1016/j.watres.2014.12.007

Ristovski, Z. D., Fletcher, C., D'Anna, B., Johnson, G. R., and Bostrom, J. T. (2006). Characterization of iodine particles with volatilization-humidification tandem differential mobility analyser (VH-TDMA), Raman and SEM techniques. *Atmos. Chem. Phys.Discuss.* 6, 1481–1508. doi:10.5194/acpd-6-1481-2006

R'Mili, B., Strekowski, R. S., Temime-Roussel, B., Wortham, H., and Monod, A. (2022). Important effects of relative humidity on the formation processes of iodine oxide particles from CH3I photo-oxidation. *J. Hazard. Mater.* 433, 128729.

Saunders, R. W., Kumar, R., Gómez Martín, J. C., Mahajan, A. S., Murray, B. J., and Plane, J. M. C. (2010). Studies of the formation and growth of aerosol from molecular iodine precursor. *Z. Phys. Chem.* 224 (7–8), 1095–1117. doi:10.1524/zpch.2010.6143

Saunders, R. W., and Plane, J. M. C. (2006). Formation pathways and composition of iodine oxide ultra-fine particles. *Environ. Chem.* 2 (4), 299–303. doi:10.1071/en05079

Sherwood, P. M. A. (1976). X-ray photoelectron spectroscopic studies of some iodine compounds. *J. Chem. Soc. Faraday Trans.* 2 (72), 1805–1820. doi:10.1039/f29767201805

Sinitsyn, D. S., Nazarov, D. A., Mosunova, N. A., and Sorokin, A. A. (2024). Model for the formation of iodine oxide nanoparticles within the reactor containment. *Therm. Eng.* 71, 941–949. doi:10.1134/s0040601524700496

Sipil¨a, M., Sarnela, N., Jokinen, T., Henschel, H., Junninen, H., Kontkanen, J., et al. (2016). Molecularscale evidence of aerosol particle formation via sequential addition of HIO3. *Nature* 537 (7621), 532–534. doi:10.1038/nature19314

Smulders, M. M. J., and Nitschke, J. R. (2012). Supramolecular control over Diels–Alder reactivity by encapsulation and competitive displacement. *Chem. Sci.* 3, 785–788. doi:10.1039/c1sc00847a

Soffer, L., Burson, S. B., and Ferrell, C. M. (1995). Accident source terms for light-water nuclear power plants. *NUREG-1465*.

Steinhauser, G., Brandl, A., and Johnson, T. E. (2014). Comparison of the Chernobyl and Fukushima nuclear accidents: a review of the environmental impacts. *Sci. Total Environ.* 470–471, 800–817. doi:10.1016/j.scitotenv.2013.10.029

Stewart, F. A., Akleyev, A. V., Hauer-Jensen, M., Hendry, J. H., Kleiman, N. J., Macvittie, T. J., et al. (2012). ICRP publication 118: ICRP statement on tissue reactions and early and late effects of radiation in normal tissues and organs–threshold doses for tissue reactions in a radiation protection context. *Ann. ICRP* 41 (1-2), 1–322. doi:10.1016/j.icrp.2012.02.001

Tang, I. N., and Castleman, Jr., A. W. (1970). Kinetics of $\gamma$-induced decomposition of methyl iodide in air. *J. Phys. Chem.* 74 (22), 3933–3939. doi:10.1021/j100716a014

Tietze, S., Kärkelä, T., and Foreman, M. R. S. J. (2012). Adsorption and revaporisation studies on iodine oxide aerosols deposited on containment surface materials in LWR, NKS-R, NKS-272.

Tsai, S. C., Wang, T. H., Wei, Y. Y., Yeh, W. C., Jan, Y. L., and Teng, S. P. (2008). Kinetics of Cs adsorption/desorption on granite by a pseudo first order reaction model. *J. Radioanal. Nucl. Chem.* 275, 555–562. doi:10.1007/s10967-007-7045-y

Vicari, L. A., de Lima, V. A., de Moraes, A. S., and Lopes, M. C. (2021). Remaining capacity estimation of lead-acid batteries using exponential decay equations. Orbital: electron. *J. Chem.* 13, 392–398. doi:10.17807/orbital.v13i5.1555

Wren, J. C., Ball, J. M., and Glowa, G. A. (2000). The chemistry of iodine in containment. *Nucl. Technol.* 129 (3), 297–325. doi:10.13182/NT129-297